earthquake can be modeled as a double couple force acting stepwise in time and pointwise in space. Such a force near Earth's surface excites fundamental spheroidal modes whose amplitudes increase with increasing frequency.

Other possibilities, including undetected aseismic events at oceanic ridges and deep-sea trenches, cannot be excluded. Analyses of horizontal component records are crucial to understanding the excitation mechanism of background free oscillations, because random atmospheric or oceanic loading will hardly excite the toroidal modes, which is likely to be excited efficiently if the source was within the solid Earth. If only the spheroidal modes were observed on the horizontal component records, then the atmospheric origin of our observed oscillations would be favored. Unfortunately, it is difficult to detect weak signals at a required level from the horizontal component records of recent global seismic networks because the records usually suffer from large amounts of low-frequency noise (*18*).

We recently analyzed the records of a superconducting gravimeter at Syowa Station, Antarctica, and obtained a spectrogram showing the vertical lines at frequencies mostly corresponding to the fundamental spheroidal modes (*19*). The lines in the superconducting gravimeter spectrogram show the following characteristics: (i) They are visible even at frequencies down to 0.3 mHz, (ii) their intensity is seasonally varying, (iii) they have high intensity at frequencies between 3 and 4 mHz, and (iv) other lines that do not correspond to seismic normal modes are present. We find no such characteristics in the IDA spectrograms. The origin of these differences is now under consideration.

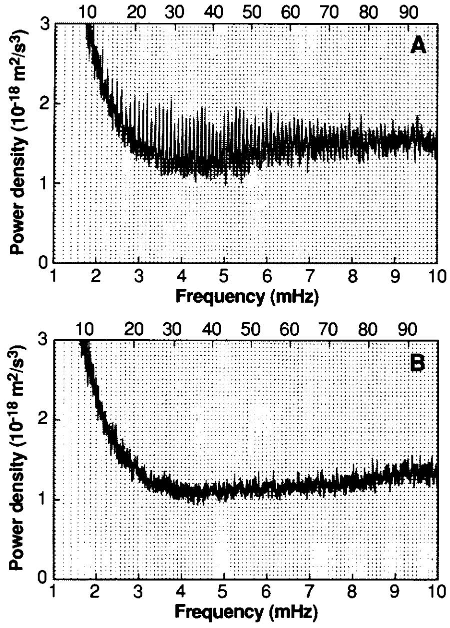

Fig. 3. Comparison of the averaged power spectral density at SUR between (**A**) the observed and (**B**) synthetic spectrograms for the seismically inactive periods, which are 437 days (12% of the total record) selected from the 10-year period. Vertical dotted lines indicate eigenfrequencies of the fundamental spheroidal modes; numbers at top indicate mode angular orders. In (A), clear spectral peaks can be seen, which are observed as the vertical lines in Fig. 1. No such clear peaks are seen in (B).

REFERENCES AND NOTES

1. G. C. Beroza and T. Jordan, *J. Geophys. Res.* **95**, 2485 (1990).
2. D. C. Agnew *et al.*, *Eos* **57**, 180 (1976).
3. R. Buland, J. Berger, F. Gilbert, *Nature* **277**, 358 (1979).
4. *Federation of Digital Seismograph Networks Station Book* (Incorporated Research Institutions for Seismology, Washington, DC, 1994).
5. D. C. Agnew *et al.*, *Eos* **67**, 203 (1986).
6. The IDA project team provides computer routines of the system response for calibrating amplitude and phase of seismic records. Uncertainty in the amplitude response is less than several percent, which does not affect our results.
7. D. C. Agnew and J. Berger, *J. Geophys. Res.* **83**, 5420 (1978).
8. Low-frequency noise at RAR is an order of magnitude larger than that at an average station.
9. A. M. Dziewonski and D. L. Anderson, *Phys. Earth Planet. Inter.* **25**, 297 (1981).
10. A. M. Dziewonski, G. Ekström, M. P. Salganik, *ibid.* **91**, 187 (1995).
11. F. Gilbert and A. M. Dziewonski, *Philos. Trans. R. Soc. London Ser. A*, **278**, 187 (1975).
12. A. R. Bulsara and L. Gammaitoni, *Phys. Today* **49**, 39 (1996).
13. Mode amplitude $A(M_o)$ is proportional to the seismic moment M_o if the attenuation effect is ignored. Let the number of earthquakes with seismic moments in a range from M_o to $M_o + dM_o$ be $n(M_o)dM_o$. According to the G-R relation, $n(M_o)$ is proportional to $M_o^{-5/3}$ if the b value is unity. Random occurrence of earthquakes with moments up to M_o contributes to the resultant amplitude as $[\int_0^{M_o} A(M_o)^2 n(M_o) dM_o]^{1/2}$, which is proportional to $M_o^{2/3}$. This means that the contribution of earthquakes with magnitudes up to M_w is only one-tenth of that of earthquakes with magnitudes up to $M_w + 1$.
14. D. J. Thomson and A. D. Chave, in *Advances in Spectrum Analysis and Array Processing*, S. Haykin, Ed. (Prentice-Hall, Englewood Cliffs, NJ, 1991), pp. 58–113.
15. R. J. Warburton and J. M. Goodkind, *Geophys. J. R. Astron. Soc.* **48**, 281 (1977).
16. T. Lay and H. Kanamori, *J. Geophys. Res.* **90**, 605 (1985).
17. N. Kobayashi, paper presented at the Fall Meeting of the Japanese Society for Planetary Sciences, Fukuoka, Japan, 4 October 1996.
18. G. G. Sorrells, *Geophys. J. R. Astron. Soc.* **26**, 71 (1971).
19. K. Nawa *et al.*, *Earth Planets Space*, **50**, 3 (1998).

18 November 1997; accepted 17 February 1998

Formation of a Magmatic-Hydrothermal Ore Deposit: Insights with LA-ICP-MS Analysis of Fluid Inclusions

Andreas Audétat,* Detlef Günther, Christoph A. Heinrich

The physical and chemical mechanism of ore precipitation in the Yankee Lode tin deposit (Mole Granite, Australia) was quantified by direct trace-element microanalysis of fluid inclusions. Laser ablation–inductively coupled plasma–mass spectrometry (LA-ICP-MS) was used to measure element concentrations in a series of fluid inclusions representing the fluid before, during, and after the deposition of cassiterite (SnO_2). Tin precipitation was driven by mixing of hot magmatic brine with cooler meteoric water. At the same time, a separate magmatic vapor phase selectively transported copper and boron into the liquid mixture.

Magmatic-hydrothermal ore deposits are a main source of Cu, W, Sn, Mo, and Au (*1*). They result from a sequence of complex geological processes beginning with the generation of hydrous silicate magmas, followed by their crystallization, the separation of volatile-rich magmatic fluids, and finally, the precipitation of ore minerals in veins or replacement deposits (*2*). A quantitative understanding of the latter two stages has been limited by a lack of information about trace-element concentrations in evolving hydrothermal fluids. Two specific questions depend on such data: (i) the role of magmatic brine-vapor separation in selective metal transport and (ii) the chemical reactions and relative importance of different physical processes leading to ore-mineral precipitation.

Experimental laboratory studies (*3*, *4*) and surface sampling of fluids from active geothermal areas and volcanic gas discharge sites have provided important information on the concentrations and solubilities of metals in hydrothermal fluids. Direct information about the nature of fluids at several kilometers depth and at temperatures as

---

Institute for Isotope Geology and Mineral Resources, ETH Zentrum NO, CH-8092 Zürich, Switzerland.

*To whom correspondence should be addressed. E-mail: audetat@erdw.ethz.ch

high as 500° to 900°C is recorded by fluid inclusions, trapped in minerals that grew at the time of ore formation and later exposed by erosion (*5*). These inclusions are typically 5 to 50 μm in size, corresponding to 10^{-11} to 10^{-8} g total mass. Microbeam spectrometry using Raman (*6*), proton-induced x-ray emission (*7*, *8*), and synchrotron–x-ray fluorescence excitation (*9*) as well as laser-ablation microsampling linked with inductively coupled plasma–mass spectrometry (ICP-MS) (*10*, *11*) or ICP–optical emission spectrometry (*12*) have been used for analysis. We show that a laser-optical system together with a high-sensitivity ICP quadrupole mass spectrometer can be designed and optimized especially for fluid inclusion analysis (*13*). We used this technique to analyze multiple generations of fluid inclusions trapped immediately before, during, and after ore-mineral precipitation in a typical Sn vein, which permitted direct evaluation of the ore-depositing mechanism.

The Yankee Lode, a small but rich magmatic-hydrothermal vein deposit in eastern Australia, is part of a classic and well-described polymetallic province zoned around the large Mole Granite intrusion (*14*, *15*). The vein mineralogy is simple, and fluid inclusions record a clear evolution of hydrothermal fluids through time. The vein contains mainly quartz and cassiterite preserved as crystals in open cavities. Wall rock alteration is minimal. The ore grade is extremely high, with Sn concentration locally as high as 20 wt %. Two selected quartz crystals show identical histories of hydrothermal growth and precipitation of other minerals, recorded by successive zones of solid inclusions within the quartz (Fig. 1A). Numerous trails of fluid inclusions represent the surrounding fluid as it was trapped at distinct stages of crystal growth. Many of these trails, of which at least 17 could be placed in an unambiguous time sequence, contain low-density vapor inclusions together with high-density brine inclusions, indicating that the fluid was boiling throughout most of the history of quartz precipitation (Fig. 1B). Microthermometric measurements were performed on both types of inclusions to obtain apparent salinities (wt % $NaCl_{equiv}$) (*16*). Pressure for each trapping stage was derived by fitting $NaCl_{equiv}$ values and homogenization temperatures (Th_{tot}) of each fluid pair into the NaCl-H_2O model system (*17*, *18*). The data show that during quartz growth, three pulses of hot fluid were injected into the vein system, each associated with a transient increase in pressure (Fig. 2A). However, it should be noted that the NaCl-H_2O model is only an approximation of the real system. In any case, the homogenization temperatures will correspond to actual trapping temperatures. The large pressure fluctuations are no doubt real, but the pressure estimates based on the model system may be significantly in error.

To reconstruct the chemical evolution of the ore-forming fluid, we selected 16 inclusion trails of known relative chronology and analyzed 48 fluid inclusions previously measured by microthermometry. Our LA-ICP-MS system uses a 193-nm ArF excimer laser (Compex 110I, Lambda Physik) with an output energy of 200 mJ. Two lens arrays produce a homogeneous, flat-top laser beam, which is imaged onto the sample surface by a diachromatic mirror in a modified petrographic microscope. The beam spot diameter can be switched instantaneously from 4 to 10, 20, 40, 60, or 80 μm during ablation, and a TV camera allows simultaneous observation of the sample (*19*). A stream of Ar gas transports the ablated material from the sample chamber into the ICP quadrupole mass spectrometer (Elan 6000, Perkin-Elmer), which has a modified interface for enhanced sensitivity and low background intensity. Up to 40 major and trace elements can be detected simultaneously as transient signals (*13*).

Element concentration ratios were calculated by referencing intensity integrals against signals from external standards (NIST612 silicate glass and aqueous solutions). These ratios were then converted to absolute concentrations using Na as an internal standard. The concentration of Na in fluid inclusions was calculated from their apparent salinity (measured by microthermometry) and the relative abundance of other major cations (from LA-ICP-MS), using empirical relations (*8*, *13*).

Early saline inclusions from the Yankee Lode have a composition that is typical of a magmatic brine. The 17 measured elements cover a concentration range from 1 to 100,000 ppm (Fig. 2) and are grouped into

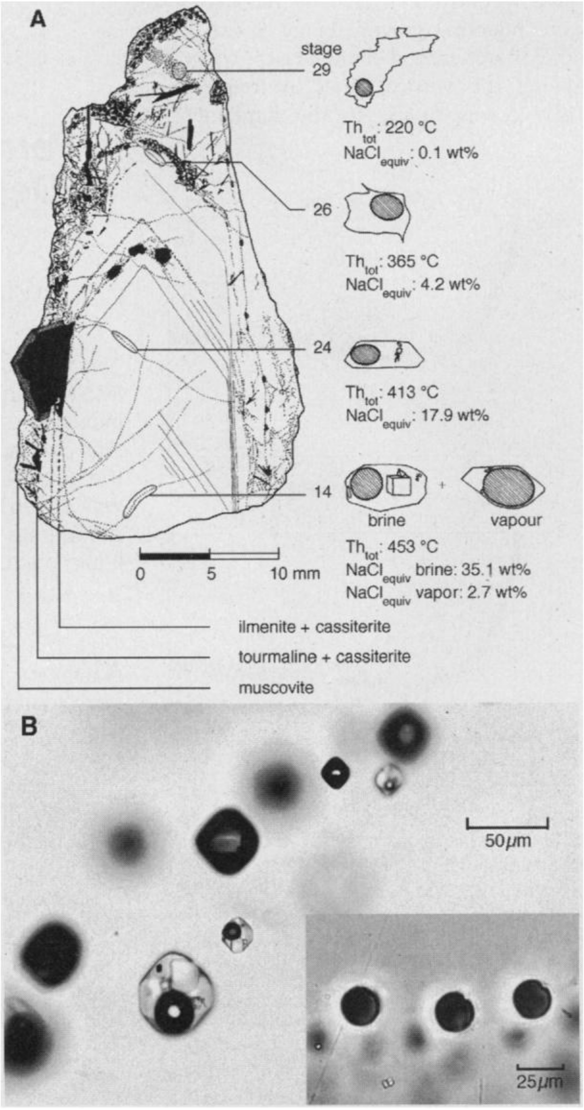

Fig. 1. (**A**) Longitudinal section through a quartz crystal from the Yankee Lode Sn deposit, showing numerous trails of pseudosecondary fluid inclusions and three growth zones recording the precipitation of ilmenite, cassiterite, and muscovite onto former crystal surfaces. The fluid inclusions shown in the right part of the figure represent four different stages in the evolution from a magmatic fluid toward a meteoric water-dominated system. Th_{tot} corresponds to the final homogenization temperature. (**B**) Photomicrograph of fluid inclusions formed by healing of a former crack within the crystal. Brine and vapor inclusions coexisting along the same trail demonstrate that the hydrothermal fluid was boiling at the time of trapping. The inset shows laser ablation craters after analysis of three inclusions.

nonprecipitating (Fig. 2B), precipitating (Fig. 2C), and volatile elements (Fig. 2D). The concentrations of most major and minor elements follow the same trend, maintaining constant concentration ratios throughout the fluid history of the vein. Concentrations are initially high and independent of fluctuations in temperature and pressure, and then drop over several orders of magnitude in later inclusions (Fig. 2B). No minerals containing any of these chemically diverse elements were precipitated anywhere in the vein at this stage. Therefore, the concentration drop either reflects a compositional evolution of the magmatic fluid (source variation) or mixing of this fluid with increasing amounts of meteoric water (dilution). Calculations based on experimental measurements (*20*) indicate that distillation effects during fluid separation from a crystallizing magma source could cause parallel variations in the concentrations of chloride-complexed metals, but the maximum realistic variation predicted by these models (∼100 times decrease in metal concentrations) is much smaller than the 5000 times decrease measured at Yankee Lode. Even a 100 times distillation effect is only possible if the pressure in the magmatic fluid source is relatively high (>150 MPa) and if the magma chamber remains perfectly mixed, neither of which is likely in the case of the Mole Granite intrusion (*4*, *21*). Mixing with meteoric water, on the other hand, is consistent with regional stable-isotope and fluid inclusion studies from the Mole Granite intrusion (*14*, *22*).

Tin, as the main precipitating ore-forming element (Fig. 2C), apparently follows a similar trend, but its concentration drops distinctly more rapidly than the nonprecipitating elements. The concentration of Sn starts to decrease exactly at the onset of cassiterite precipitation, as recorded by the first growth zone containing this mineral. By stage 23 of the fluid-trapping history, the Sn concentration has dropped to only 5% of its initial value, even though the nonprecipitating elements show that the fluid mixture at that stage still contains 35% magmatic fluid. This directly demonstrates that the chemical and thermal effect (cooling) of fluid mixing was the cause for cassiterite precipitation. The precipitation efficiency can be calculated as 86% of the initial amount of Sn that was contributed to the fluid mixture that is recorded by inclusions from stage 23. Thermodynamic models, designed to compare the efficiency of alternative mechanisms for cassiterite precipitation in magmatic-hydrothermal systems, also indicate that fluid mixing is more efficient in terms of cassiterite enrichment than the two main alternatives, fluid-rock reaction or vapor separation (*23*). Fluid-rock reaction is able to produce low-grade deposits only, and the association at Yankee Lode of very high ore grades in veins with practically no wall-rock alteration rules out this possibility. Vapor separation indeed was associated with cooling and decompression at Yankee Lode, but was probably not the cause for cassiterite deposition, because the magmatic fluid underwent three cycles of cooling and boiling before saturation of cassiterite occurred in a third cycle at the onset of fluid mixing.

The first marked reduction in the concentration of B (Fig. 2D) at stage 25 matches exactly the precipitation of tourmaline. But despite significant dilution of all nonprecipitating elements, the B concentration remained near its original magmatic value through stages 23 and 24, and decreased less

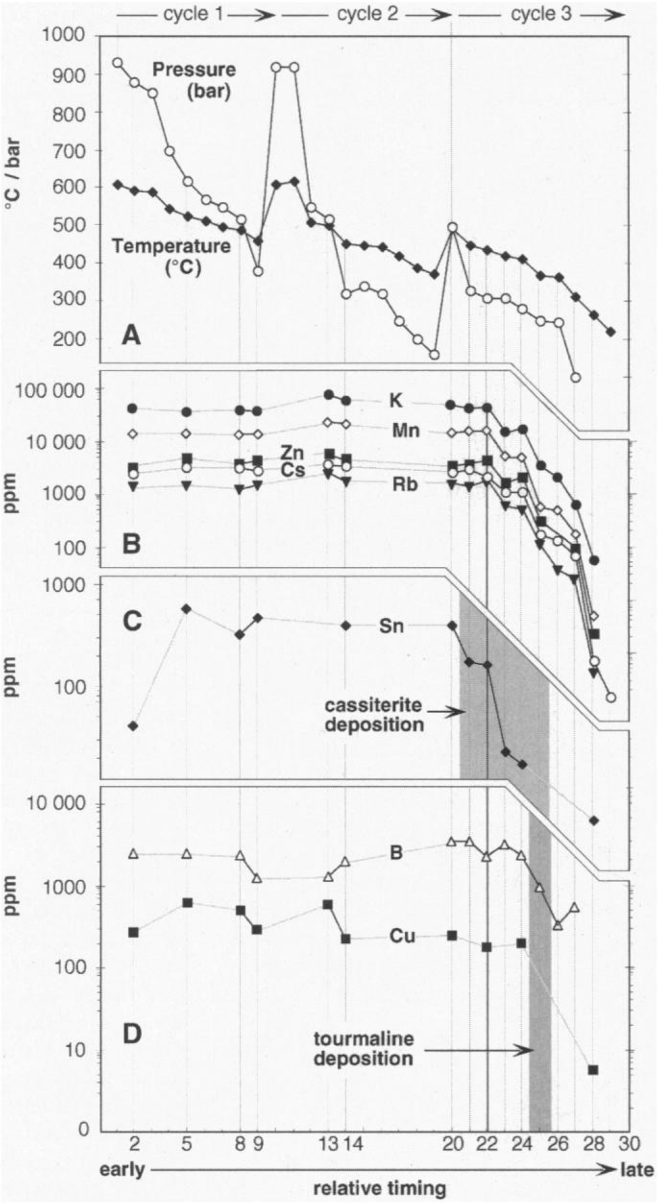

Fig. 2. Evolution of pressure, temperature, and chemical composition of the ore-forming fluid, plotted on a relative time scale recorded by the growing quartz crystal. (**A**) Variation in temperature and pressure, calculated from microthermometric data. Hot, magmatic fluid was introduced into the vein system in three distinct pulses before it started to mix with cooler meteoric groundwater. (**B**) Concentrations of nonprecipitating major and minor elements in the liquid-dominant fluid phase, interpreted to reflect progressive groundwater dilution to extreme values. (**C**) A sharp drop in Sn concentration is controlled by the precipitation of cassiterite. (**D**) B and Cu concentrations reflect not only mineral precipitation (tourmaline) but also the selective enrichment of the brine-groundwater mixture by vapor-phase transport.

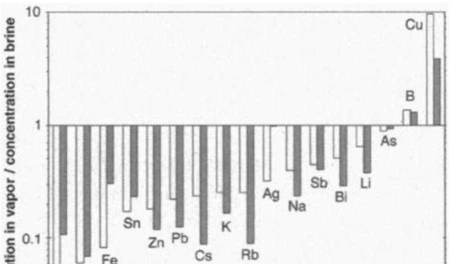

Fig. 3. Partitioning of 17 elements between magmatic vapor and coexisting brine, calculated from analyses of four vapor and nine brine inclusions in two "boiling assemblages." At both pressure and temperature conditions recorded in these assemblages, Cu and B strongly fractionate into the magmatic vapor phase.

markedly through stages 26 and 27, even though tourmaline was growing and extracting B from the fluid. Similarly, Cu decreased by only a factor of 40 between stages 22 and 28, even though the nonprecipitating elements show a dilution factor as high as 1300. This observation of apparent Cu and B excess is readily explained by condensation of magmatic vapor into the mixing liquids. The vapor phase of coexisting vapor and brine inclusions was found to be selectively enriched in these two elements compared with the brine. Distribution coefficients, $D = M_{vapor}/M_{liquid}$, were calculated for two sets of fluid pairs (Fig. 3). Both show a similar fractionation pattern: strongly chloride-complexed elements partition in favor of the saline liquid, whereas B and Cu partition preferentially into the vapor phase. Copper is enriched in the vapor phase by a factor up to 10, and concentration ratios of Cu to other first-row transition metals exceed the corresponding ratios in the brine by a factor of 100 to 500. High concentrations of Cu have been known from volcanic gas inclusions (*24*), but earlier evidence for strong metal partitioning between coexisting brine and vapor had been ambiguous (*8*, *25*). We suggest that some copper(I) bisulfide complexes may stabilize Cu in the S-enriched vapor phase (*8*), in contrast to most other metals which are held in the brine by stable chloro complexes (*3*). The same chemical behavior would be expected for Au(I), which could be a key factor in the selective enrichment of this element with Cu and As in high sulfidation epithermal deposits.

The fluid inclusion microanalyses also constrain the physical processes of hydrothermal ore formation. Two pulses of magmatic fluid, each associated with an increase in fluid temperature and pressure, passed through the vein system before meteoric groundwater reached the site of the growing quartz crystals and caused Sn precipitation. For the observed metal concentration of up to 20 wt % Sn in the Yankee Lode to be produced, ~500 m^3 of magmatic brine (containing ~400 ppm Sn) must have flowed through 1 m^3 of vein, precipitating all its dissolved Sn within this volume by mixing with ~10^6 m^3 of meteoric water. For the two fluids to always mix at the same place for an extended period of time, a stable plumbing system is required. This may either be attained at the interface between two overlying convection cells or by mixing of magmatic fluid ascending in one vein with meteoric water penetrating from a cross-cutting vein. The latter case is consistent with the evidence that many deposits in the Mole Granite intrusion and elsewhere contain exceptionally rich ore shoots at the intersection of two fluid channelways (*26*).

REFERENCES AND NOTES

1. S. E. Kesler, *Mineral Resources, Economics and the Environment* (Macmillan, New York, 1994).
2. J. W. Hedenquist and J. B. Lowenstern, *Nature* **370**, 519 (1994).
3. T. M. Seward and H. L. Barnes, in *Geochemistry of Hydrothermal Ore Deposits*, H. L. Barnes, Ed. (Wiley, New York, ed. 3, 1997), pp. 435–477.
4. P. A. Candela and P. M. Piccoli, in *Magmas, Fluids, and Ore Deposits*, J. F. H. Thompson, Ed. (*Short Course Series 23*, Mineral Association of Canada, Victoria, British Columbia, 1995), pp. 101–127.
5. E. Roedder and R. J. Bodnar, in (*3*), pp. 657–698.
6. J. Dubessy, B. Poty, C. Ramboz, *Eur. J. Mineral.* **1**, 517 (1989).
7. C. G. Ryan *et al.*, *Nucl. Instrum. Methods Phys. Res. B* **54**, 292 (1991).
8. C. A. Heinrich, C. G. Ryan, T. P. Mernagh, P. J. Eadington, *Econ. Geol.* **87**, 1566 (1992).
9. J. A. Mavrogenes *et al.*, *Geochim. Cosmochim. Acta* **59**, 3987 (1995).
10. T. J. Shepherd and S. R. Chenery, *ibid.*, p. 3997.
11. R. R. Loucks, J. A. Mavrogenes, W. Hibberson, *Geol. Soc. Aust. Abstr. Ser.* **41**, 258 (1996).
12. M. C. Boiron *et al.*, *Geochim. Cosmochim. Acta* **55**, 917 (1991).
13. D. Günther, A. Audétat, R. Frischknecht, C. A. Heinrich, *J. Anal. Atom. Spectrom.*, in press.
14. P. J. Eadington, *Econ. Geol.* **78**, 1204 (1983).
15. C. A. Heinrich and C. G. Ryan, in *Water-Rock Interaction*, Y. K. Kharaka and A. S. Maest, Eds. (Balkema, Rotterdam, 1992), pp. 1583–1587.
16. R. J. Bodnar and M. O. Vityk, in *Fluid Inclusions in Minerals: Methods and Applications*, B. De Vivo and M. L. Frezzotti, Eds. (Virginia Polytechnic Institute and State Univ. Press, Blacksburg, VA, 1994), pp. 117–130.
17. R. J. Bodnar, C. W. Burnham, S. M. Sterner, *Geochim. Cosmochim. Acta* **49**, 1861 (1985).
18. J. L. Bischoff and K. S. Pitzer, *Am. J. Sci.* **289**, 217 (1989).
19. D. Günther, R. Frischknecht, C. A. Heinrich, H. J. Kahlert, *J. Anal. Atom. Spectrom.* **12**, 939 (1997).
20. J. S. Cline and R. J Bodnar, *J. Geophys. Res.* **96**, 8113 (1991).
21. J. D. Kleeman, in *New England Geology*, P. G. Flood and B. Runnegar, Eds. (University of New England, Armidale, Australia, 1982), pp. 327–334.
22. S. S. Sun and P. J. Eadington, *Econ. Geol.* **82**, 43 (1987).
23. C. A. Heinrich, *ibid.* **85**, 457 (1990).
24. J. B. Lowenstern, G. A. Mahood, M. L. Rivers, S. R. Sutton, *Science* **252**, 1405 (1991).
25. A. H. Damman *et al.*, *Eur. J. Mineral.* **8**, 1081 (1996).
26. C. S. J. Mulholland, in *Geology of Australian Ore Deposits*, A. B. Edwards, Ed. (Australian Institute of Mining and Metallurgy, Melbourne, 1953), vol. 1, pp. 944–949.

27. We thank U. Menet for help with the engineering and construction of the laser ablation system and the modification of the ICP-MS, R. Frischknecht who assisted us during its operation, P. Ashley, J. Stroud, and H. Henley for field support, and J. Ridley and T. Seward for reading through the manuscript and giving critical comments.

16 December 1997; accepted 13 February 1998

Siliceous Tablets in the Larval Shells of Apatitic Discinid Brachiopods

Alwyn Williams,* Maggie Cusack, James O. Buckman,
Thomas Stachel

The marine bivalved Brachiopoda are abundant throughout the geological record and have apatitic ($CaPO_4$-rich) or calcitic ($CaCO_3$-rich) shells. Vesicles covering the larval valves of living apatitic-shelled discinids contain tablets of silica. The tablets are cemented into close-packed mosaics by spherular apatite in glycosaminoglycans. They are usually lost as vesicles degrade but leave imprints on the underlying apatitic shell. Similar imprints ornament larval surfaces of some of the earliest Paleozoic apatitic-shelled brachiopods and may also be indicators of siliceous biomineralization.

The composition of shells of living and extinct marine bivalved Brachiopoda has been regarded as apatitic ($CaPO_4$) or calcitic ($CaCO_3$) (*1*). The shell of the subconical mature discinid brachiopods consists of an outer chitino-proteinaceous coat (periostracum), several micrometers thick, underlain by laminar layers composed of the carbonate fluorapatite, francolite $[Ca_{10}(PO_4)_5CO_3F_{1.5}(OH)_{0.5}]$, and organic compounds (*2*). The apatite occurs as protein-coated granules, 4 to 8 nm in diameter, aggregated into spherules, 30 to 150 nm in size, that are either compacted into laminae or further aggregated into mosaics or rods immersed in glycosaminoglycans (GAGs) (*3*) and supported by proteinaceous strands or mats of β-chitin (*2*).

In *Discinisca tenuis*, the coat secreted by the larval epidermis is preserved as a pair of circular patches, about 500 μm in diameter, at the apices of mature valves. The larval valves are delineated by a raised margin (Fig. 1A) and are covered with close-packed vesicles (*4*) containing biomineralized tablets (*2*), about 70 nm thick, which are hexagonal, rhombic, or ditetragonal in outline and virtually of constant size with major axes averaging 1.3 μm (Fig. 1, B and C). The tablets were separated from the larval shell surfaces (*5*) and their composition estimated by energy-dispersive x-ray (EDX) spectra on a scanning electron mi-

---

A. Williams and J. O. Buckman, Palaeobiology Unit, University of Glasgow, Glasgow G12 8QQ, UK.
M. Cusack, Department of Geology and Applied Geology, University of Glasgow, Glasgow G12 8QQ, UK.
T. Stachel, Institute of Mineralogy, Johann Wolfgang Goethe-University, Frankfurt D-60054, Germany.

*To whom correspondence should be addressed.